ADVANCED MATERIALS
www.advmat.de

Materials Views
www.MaterialsViews.com

Renewable-Juglone-Based High-Performance Sodium-Ion Batteries

Hua Wang, Pengfei Hu, Jie Yang, Guangming Gong, Lin Guo, and Xiaodong Chen*

Currently, existing energy-storage devices built with man-made electrode materials exhibit substantial energy density, however, suffer from poor biocompatibility, safety hazard, rising prices, and cause numerous electronic wastes after service life.[1–15] Next-generation green and sustainable energy systems with high energy density will dominate the future human life, of which renewable-biomass-based electrodes should be a promising class of candidates.[16–27] Inspired by the metabolic process resided in organisms relying on ions transport and energy exchanges of biomolecule with specific functional groups such as carbonyl groups,[28,29] carboxyl groups,[30,31] and amino groups,[32–35] man-made organic materials with redox centers have been investigated to fabricate advanced energy-storage devices. For instance, electrons and protons, as well as sodium ions or lithium ions, could be stored and transferred through the use of versatile redox-active functionalities, and related supercapcitors, and sodium/lithium-ion batteries have been intensively studied.[26–33] Nevertheless, directly natural-derived redox biomolecules have been rarely involved.[34,35] Biomolecule-based electrodes are not only renowned to be renewable, abundant, sustainable, and biodegradable, but also possesses promising electrochemical performance with structural flexibility and chemical diversity, representing an attractive and emerging paradigm in versatile electronic devices, especially for biomedical implants and edible energy-storage applications.[28,29,32–37]

As organic materials, biomolecule-based electrodes possess beneficial properties of lightweight and easy processing, but they are subjected to capacity fading due to their dissolution into organic electrolytes and poor rate capacity owing to low conductivity, restricting their practical application in energy storage.[38–40] Several approaches have been adopted to overcome the dissolution and low conductivity issues of organic materials such as immobilization on specific substrates through van der Waals or hydrogen-bonding interactions, π–π stacking or electrostatic interactions,[29,33,41,42] polymerization of active compounds,[38,43–45] employing solid or quasi-solid electrolytes,[46,47] and chemical modification.[48,49] Furthermore, sodium-ion batteries with considerable energy density have been highlighted as an intriguing candidate for next-generation energy-storage systems owing to the potential cost advantage stemming from abundant natural supply, although they suffer from the poor kinetics of sodium-ion insertion and extraction due to the relatively larger radius compared with the lithium ions.[50–53] Biomolecules with redox centers possess structural flexibility ascribed to their less rigid structure with respect to inorganic materials, providing a higher mobility of sodium ions.[54,55] Thus, the successful fabrication of rechargeable sodium-ion batteries based on renewable natural-derived biomolecules, which have considerable capacity and cyclic stability, via proper strategies, is of intense expectation with scientific and technological significance.

Herein, we present a biomolecule-based electrode through a facile and scalable self-assembly process directly, without any binder or additional conductive agent. Juglone, a renewable biomolecule derived from waste walnut epicarp, is immobilized onto reduced graphene oxide (RGO) nanosheets owing to the strong π–π interaction between the aromatic structure and the carbon scaffold.[56–60] Combining the redox activities of the quinone groups in the Juglone and the high electrical conductivity of the RGO nanosheets, the renewable hybridized electrode exhibits a high storage capacity and cyclic stability in sodium-ion energy-storage devices. Furthermore, this unique method can be applied to fabricate Juglone/RGO electrodes of arbitrary size and shape with relatively high resolution and alignment accuracy on specified substrates, indicating potential applications in complex and precise fabrications of prospective advanced device architectures.

First, the Juglone/RGO composite electrode was prepared via a facile synchronous reduction and assembly method by directly immersing Cu foils into the Juglone and graphene oxide (GO) mixed solution. Followed by further reduction with hydrazine vapor, an integrated, black and rough film grown directly on a copper substrate was obtained (**Scheme 1**). **Figure 1**a and b represent a typical Juglone/RGO hybridized electrode with an area of 20 cm^2, which is flexible, as the hydroxyl groups of Juglone molecule enhance the mechanical properties of the RGO sheets. Thermodynamically, the redox potential of GO is found to be in the range of 0.4–0.6 V[61] and that of Juglone molecule is around 0.4 V, so specific metals ($\varphi_{Cu^{2+}/Cu}$ = 0.337 V) with redox potential below 0.4 V can reduce both GO and Juglone spontaneously. The morphology and structure of Juglone/RGO composite electrode were investigated by electron microscopy. The hybridized organic film with a thickness of 60 μm is grown on the copper substrate firmly (Figure 1c,d). Juglone recrystallizes and assembles into microrods wrapped with gauzy RGO nanosheets, which differs from original Juglone bulk particles before dissolution (Figures S1 and S2, Supporting Information). Figure 1e shows the RGO sheets possess a thin layered structure with few thinner ripples and overlap

Dr. H. Wang, P. Hu, J. Yang, G. Gong, Prof. L. Guo,
School of Chemistry and Environment
Beihang University
Beijing 100191, P.R. China
E-mail: guolin@buaa.edu.cn
Prof. X. Chen
School of Materials Science and Engineering
Nanyang Technological University
Nanyang Avenue, Singapore 639798, Singapore

DOI: 10.1002/adma.201405904

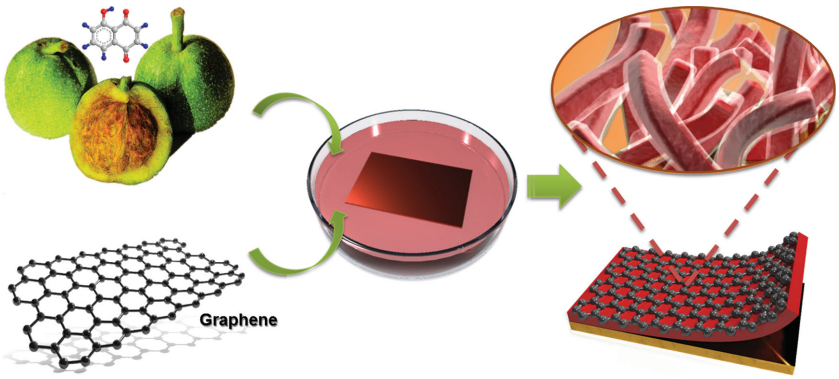

Scheme 1. Fabrication process of Juglone/RGO electrodes.

each other. The crystal structures of RGO and Juglone were characterized by the mixed ring and hexagon-spot pattern depicted in the selected area electron diffraction (SAED), and the rearranged 1D Juglone proved the well-defined crystalline structure (Figure 1f). Furthermore, the composite exhibits increased interlayer distance compared to pure RGO, indicating strong interaction effect between hybridized RGO nanosheet and Juglone molecule, which is favorable for the sodium-ion insertion (Figure S3, Supporting Information).

To further study the electronic structure of the hybridized electrode in detail, optical and photoelectron spectroscopy were utilized to analyze the interaction effect between Juglone and RGO (**Figure 2**). The Raman bands of graphene are strongly sensitive to the electronic structure and prove to be an essential tool for characterizing chemical doping or charge transfer. The blueshift of the G band with the peak around 1580 cm^{-1} in the Raman spectra demonstrates the strong π–π stacking effect, which accounts for the immobilization of Juglone molecules on RGO sheets (Figure 2a).[33,62] With the increasing mass fraction of Juglone, the stronger charge-injection effect results in a decrease of the I_g/I_d ratio and an increase of the full width at half-maximum (FWHM) of the G band.[28] The existence of Juglone molecules on RGO nanosheets was also proved by Fourier transform IR (FTIR) spectra with the appearance of peaks at 1650, 1411, and 1230 cm^{-1}, representing the introduction of quinone carbonyls (Figure S4, Supporting Information).[44] The peak at 1590 cm^{-1} (C=C stretching) shifts to higher frequencies with increasing content of Juglone owing to the enhanced interaction effect within the composite (Figures 2b and Figure S5, Supporting Information).[63] The recombination of RGO and Juglone was further monitored by X-ray photoelectron spectroscopy (XPS), as shown in Figure 2c, which confirmed the π–π conjugation of the hybridization. The C 1s spectra of C=C/C–C, C–O, and C=O are observed at 284.4, 286.9, and 288.9 eV, respectively.[64,65] The apparent negative shift of the C=O binding energy peak is attributed to electronic effect of the Juglone's phenyl group and RGO.[66,67] Simultaneously, the binding energy of the O 1s peak is shifted down and the ratio of the deconvoluted peaks changes as the content of carbonyl oxygen with the peak at 310 eV increases obviously. The above multiple spectroscopic analyses of the hybridized electrode unequivocally reveal Juglone and RGO strongly interact with each other instead of being a simple physical mixture, enhancing its stability toward organic solvents and electronic conductivity, which should result in excellent electrochemical performance in energy-storage applications.

As a proof-of-concept, a sodium-ion battery based on the as-prepared composite electrode was fabricated. Being a biomolecule with well-defined redox couples, Juglone exhibits a

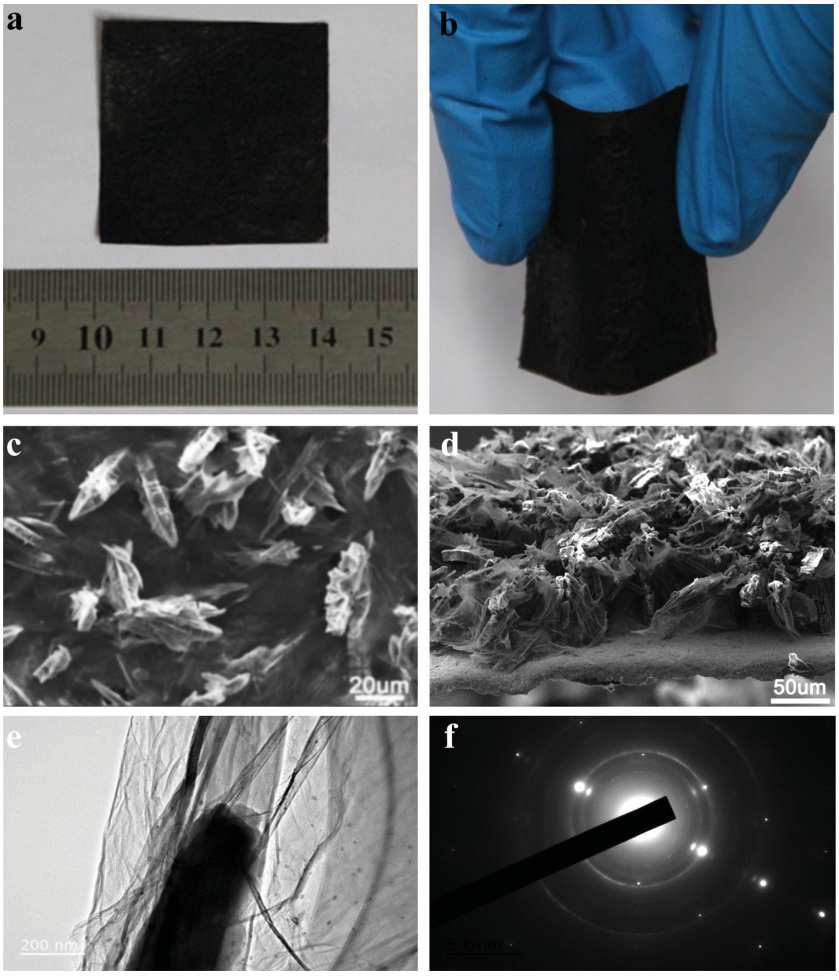

Figure 1. a,b) Photographs of a flexible Juglone/RGO electrode oncopper substrate (a,b). c,d) Typical top (c) and cross-sectional (d) view SEM images of Juglone/RGO electrodes. e,f) The TEM image (e) and SAED pattern (f) of Juglone/RGO composites.

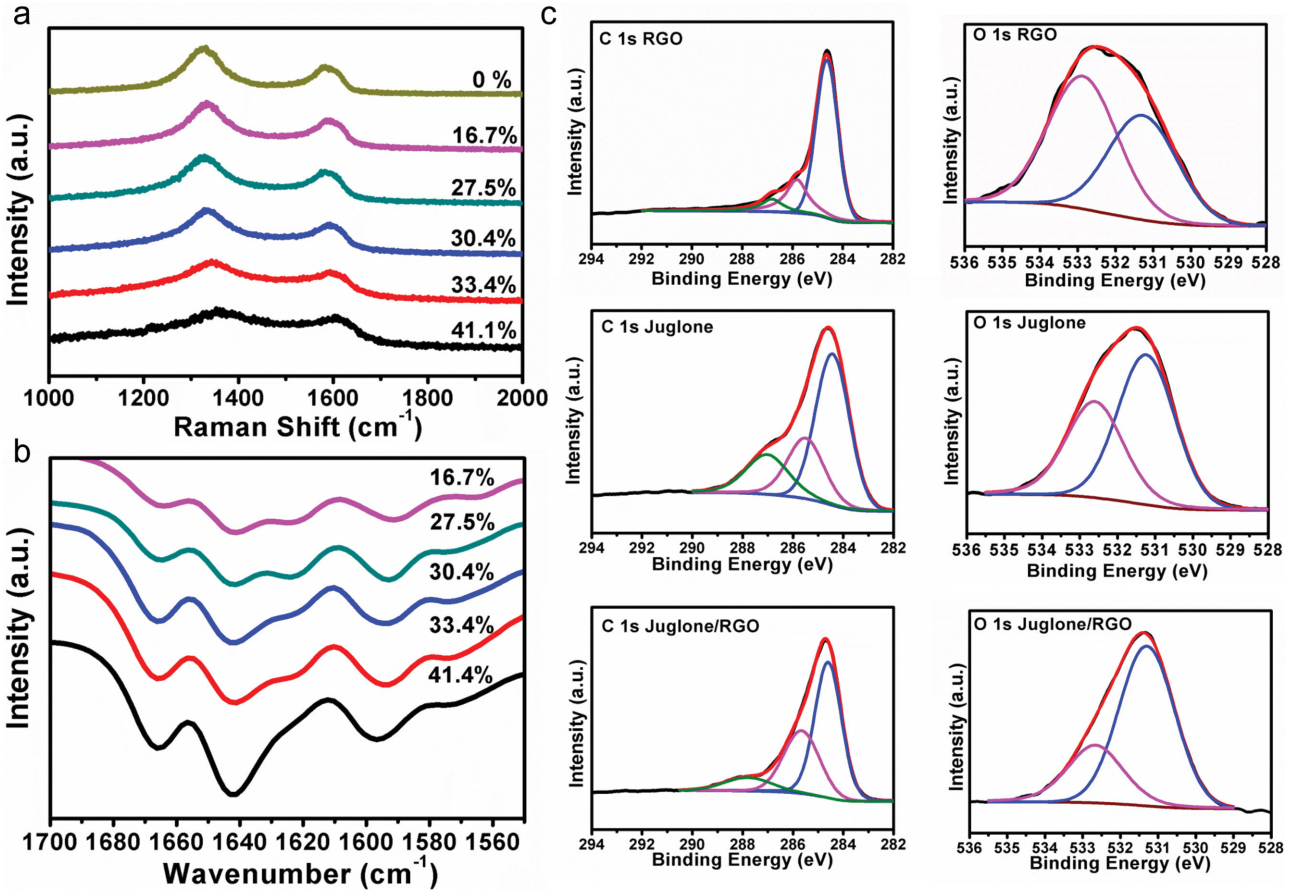

Figure 2. Raman (a) and FTIR (b) spectra of Juglone/RGO composites with different mass fractions. c) High-resolution XPS spectra of C 1s and O 1s regions of RGO, Juglone and Juglone/RGO.

superb electrochemical performance in reversibly transferring protons or sodium ions when tested in a three-electrode system (**Figure 3**a). A symmetric pair of redox peaks in the cyclic voltammetry (CV) curves is observed, indicating the electrochemical intercalation/deintercalation of the sodium ions is completely reversible. The polarization is 0.1 mV and infinitesimally changes as the scan rate increases from 5 to 25 mV s^{-1}, suggesting promising potential for high-rate batteries or supercapacitors. Nevertheless, Juglone-based electrodes suffer from the common problems of conventional organic electrodes including low cycling performance owing to the dissolution of active materials in organic electrolyte and poor capacity at high current rate ascribed to the low electroconductibility. Conjugating with RGO sheets provides an effective solution, and the as-obtained Juglone/RGO films on a copper substrate prove to be a remarkable anode without any binder or additional conductive agent when tested in a CR2032 coin-type half-cell. Based on the specific capacities of the hybridized electrodes with different mass fraction of Juglone, 30.4% was selected to be further studied (Figure S5 and S6, Supporting Information). A pair of distinctive cathodic and anodic peaks is observed with potentials of 0.6 and 1.5 V according to the CV curves of Juglone/RGO composite, which implies a different sodium storage mechanism as compared with raw Juglone or RGO electrodes (Figure 3b). A pronounced cathodic peak occurs at around 0 V in the CV curves of RGO, whereas no anodic peak is found in the reverse cycle, indicating the insertion of sodium ions between the graphene layers, similar to many other carbonaceous materials. In addition, during the first charge/discharge cycle, a weak hump occurs from 1.1 to 1.4 V and the specific capacity is 440 and 760 mA h g^{-1}, which arises from irreversible electrolyte decomposition at the electrode/electrolyte surface to form the solid-electrolyte interphase (Figure S7, Supporting Information). In accord with CV evidence, the discharge/charge voltage profile of the Juglone/RGO electrode exhibits relatively obvious plateaus and enhanced capacity (Figure 3c). Initially, the specific capacity of the Juglone/RGO cathode slightly reduces and stabilizes at 305 mA h g^{-1} after 10 cycles at a current rate of 0.1 A g^{-1}, which significantly surpasses the 40 mA h g^{-1} of the raw Juglone electrode or the 110 and 123 mA h g^{-1} of the RGO electrode (Figure 3d and Figure S8, Supporting Information). After 100 cycles, the highly reversible capacity of 280 mA h g^{-1} is stably maintained with a Coulombic efficiency of ≈99% and 212 mA h g^{-1} is retained even after cycling up to 300 times (Figure S9, Supporting Information). The rate performance is further investigated as shown in Figure 3e. The average discharge capacities of 398, 305, 250, 225, and 210 mA h g^{-1} are achieved at different current densities of 0.05, 0.1, 0.2, 0.3, and 0.4 A g^{-1}, respectively. As expected, the average capacity can recover to 350 mA h g^{-1} when the

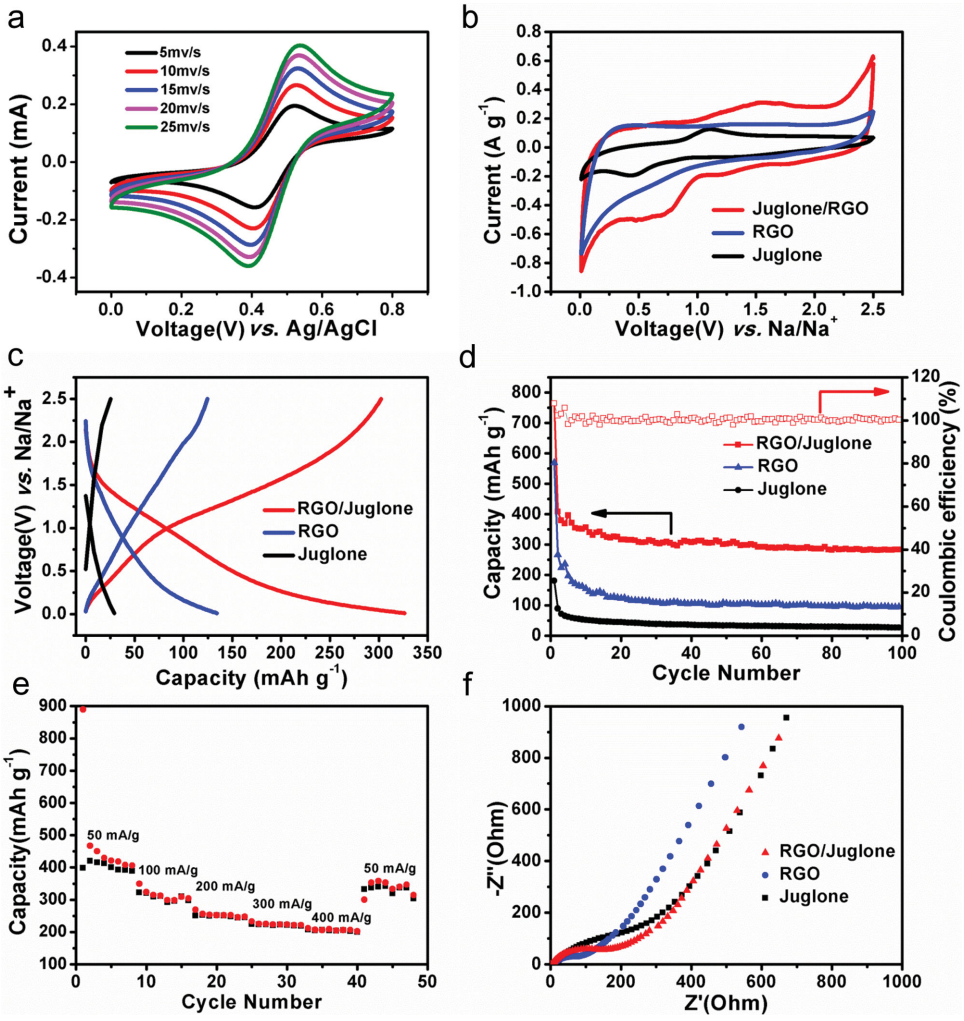

Figure 3. a) CV curves of Juglone in a mixed solution of acetonitrile/deionized water captured by a three-electrode system using Pt foils as both the counter and working electrodes, Ag/AgCl as the reference electrode, and 1 M $NaClO_4$ as the electrolyte. b–f) Electrochemical properties of Juglone/RGO electrode compared with RGO and Juglone electrodes evaluated using a half cell with sodium metal: b) CV curves at a scan rate of 1 mV s^{-1}; c) capacity–voltage profiles at 0.1 A g^{-1}; d) capacity retention at 0.1 A g^{-1}; e) rate capability; and f) electrochemical impedance spectra.

current finally reduces to 0.05 A g^{-1}, exhibiting a superior rate capability ascribed to the structural stability and enhanced electronic conductivity. The electrochemical impedance spectroscopy (EIS) spectra in Figure 3f reveal the relatively faster charge-transfer kinetics and electronic responses with lower resistance in the Juglone/RGO electrode compared with the raw Juglone electrode, solidly confirming its excellent electrochemical performance.

Probing deeper, X-ray absorption near edge spectroscopy (XANES) of the hybridized electrode was analyzed for as prepared, fully discharged and fully charged states to unveil the mechanism of sodium-ion insertion and extraction with superb resolution (**Figure 4**a). The O K-edge XANES spectra of the as-prepared electrodes exhibit a sharp

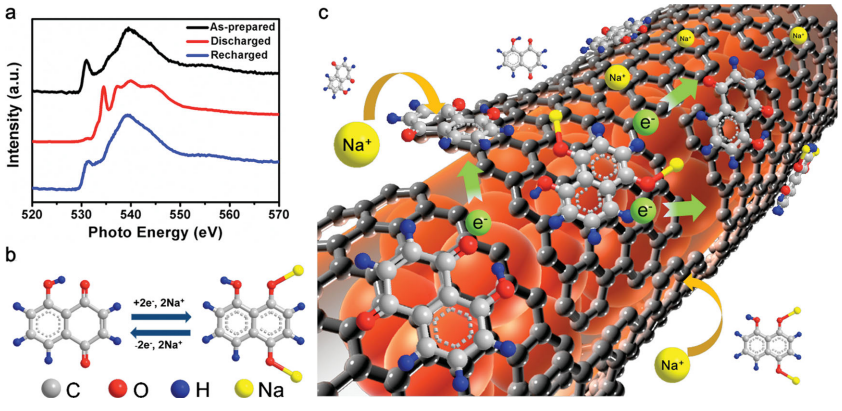

Figure 4. a) O K-edge XANES spectra of Juglone/RGO electrodes for as prepared, fully discharged and fully charged states. b) Electrochemical redox reaction mechanism of sodium ions with Juglone molecule. c) Schematic diagram for the π–π interaction of the Juglone molecule with RGO nanosheets and the reversible sodium-ion de-/insertion mechanism, as well as electron transfer of the hybridized electrodes.

spectral peak at 532 eV and a broad absorption in the range of 536–550 eV, corresponding to π^* excitation originating from C=O groups, mainly from Juglone, and σ^* excitation stemming from various C–O or C=O groups, respectively (Figure S10, Supporting Information).[68,69] After discharge, an additional sharp peak evolves at 534 eV obviously, while the C=O peak at 532 eV decreases correspondingly, which can be assigned to the formation of C–O–Na with sodium-ion insertion.[70] For a recharged electrode, the reversible diminution of the C–O–Na peak at 534 eV, as well as restoration of the peak at 532 eV is observed, which is in accordance with the redox reaction of Juglone with sodium ions. In theory, a single Juglone molecule can take up and release two Na atoms reversibly, leading to the theoretical capacity of 290 mA h g^{-1} (Figure 4b). Non-covalence immobilization of the biomolecule through π–π stacking with RGO nanosheets, which act as protective layers to suppress the dissolution problem, as well as conductive paths to realize fast charge transfer, contribute to improving the electrochemical performance of the Juglone dramatically (Figure 4c). In addition, RGO has been reported as an intrinsic carbonaceous anode for sodium/lithium batteries with considerable capacity.[64,71–75] The larger interlayer distances due to the interaction effect with Juglone here would facilitate accommodating more sodium ions and further improve the specific capacity and cycle stability. Hence, it is the synergetic effect of RGO and Juglone that accounts for the enhanced capacity, improved rate capability, and cyclability of the renewable hybridized electrodes.

Furthermore, this facile and scalable method can be applied to fabricate various Juglone/RGO electrodes of arbitrary size and shape on specified substrates, suggesting potential applications in diverse device architectures. As shown in **Figure 5**a,b, a subtle electrode was obtained using microscale copper grids as the substrate, composed of a 10-μm-wide copper line along with a 50-μm-wide gap, which can be precisely covered with Juglone/RGO films. Meanwhile, a large piece of Juglone/RGO electrode with the area of 900 cm^2 on copper foil can also be successfully fabricated (Figure 5c). Direct fabrication of size-controlled electrodes without additional binder or conductive agent, regardless of tedious slurrying and coating procedure, offers convenience for assembling batteries, especially for large-area ones. To prove the concept, an aluminum-pouch-type full sodium batteries were assembled, with this large-area binder-free Juglone/RGO electrode as the anode and a home-made $Na_3V_2(PO_4)_3$/C electrode[76] (Figure S11, Supporting Information) as the cathode, and the corresponding electrochemical performance was further investigated (Figure S12, Supporting Information). The well-defined redox peaks at 1.3/1.85 V (Figure 5e) indicate well-behaved electrode kinetics of both electrodes and exceptional sodium-ion storage abilities, and the obtained high current is capable of strongly powering an electric-fan (Figure 5d). In addition, the reversible discharge capacity could be stably retained at 80 mA h g^{-1} at a current density of 0.1 A g^{-1} even after 100 cycles, showing the potential practical application of renewable-Juglone-based sodium batteries (Figure 5f).

In summary, we have demonstrated that renewable-Juglone biomolecules with well-defined redox-active quinone carbonyl groups exhibit promising electrochemical performance in reversibly transferring sodium ions. A rational design of Juglone/RGO hybridized electrodes is proposed for the first time through a facile and scalable self-assembly approach, without additional binder or conductive agent. Analysis of optical and photoelectron spectra reveal non-covalent

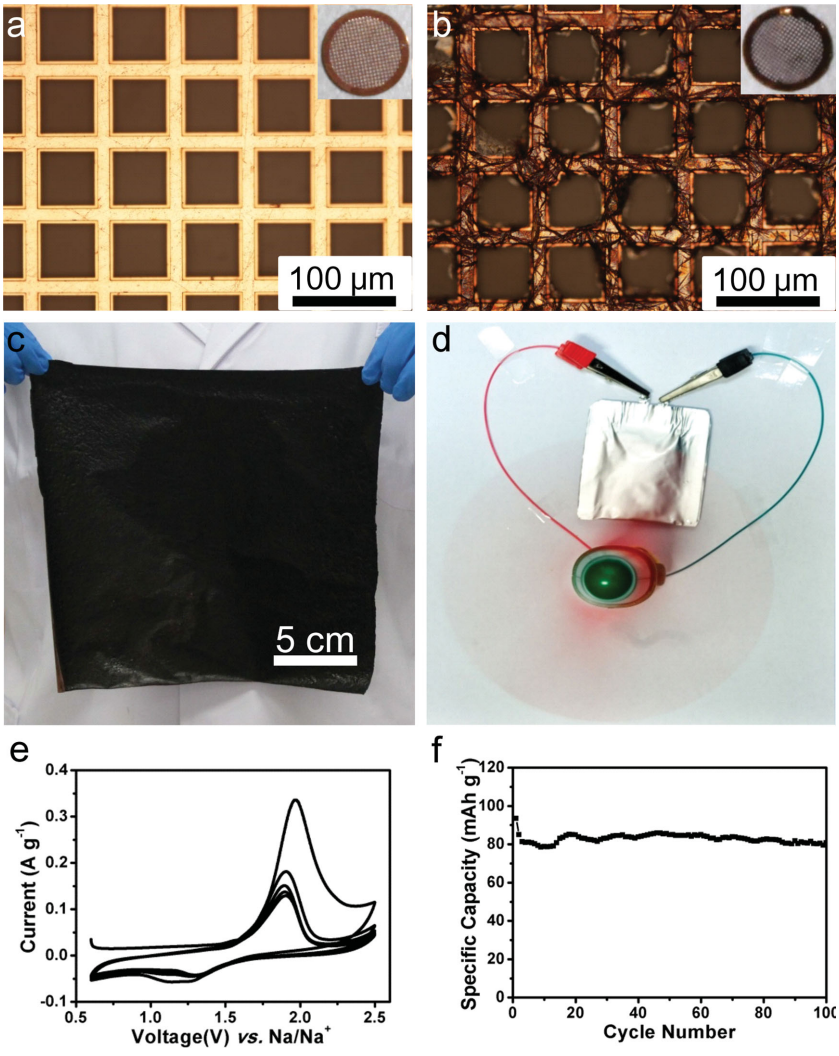

Figure 5. a,b) Optical microscopy images of copper grid (a) and patterned Juglone/RGO film (b). The insets in (a) and (b) show corresponding photographs. c,d) Photographs of a large piece of Juglone/RGO film with an area of 900 cm^2 (c) and an aluminum-pouch-type full battery used to power an electric fan (d). e,f) CV curves (e) and cycle performance (f) of a sodium-ion full battery with a Juglone/RGO electrode as the anode and a $Na_3V_2(PO_4)_3$/C electrode as the cathode.

immobilization of the redox molecules via π–π interactions on the RGO carbon scaffold, which suppresses the dissolution puzzle of organic materials and enhances both the conductivity and sodium-ion accessibility of the electrode. The sustainable biomolecule-based electrodes exhibit superior energy-storage properties such as specific capacity, cyclic stability, and rate capability. A high gravimetric capacity density up to 305 mA h g^{-1} is achieved and retains 280 mA h g^{-1} after 100 cycles. Additionally, this versatile approach can be applied to fabricate electrodes of arbitrary size and shape with relatively high resolution and alignment accuracy on specified substrates, indicating potential applications in complex and precise fabrications of prospective biocompatible electronic devices. Thus, the renewable-biomaterial-based high-performance electrodes will hold a place in the future of next-generation energy-storage devices.

Experimental Section

Preparation of Juglone/RGO Electrodes: GO was synthesized from natural graphite by a modified Hummers method. First, Juglone powders and 3 mL of GO aqueous solution (7 mg mL^{-1}) were added into a mixed solution of acetonitrile/deionized water (17 mL, 12:5, v/v), followed by continuous sonication for 5 h to form a stable suspension. Subsequently, the copper foil (or coins, copper grid) was immersed into the suspension for 24 h and a black film on the metal substrate was obtained. The film was then carefully rinsed with deionized water and reduced with hydrazine vapor under 90 °C for 8 h, followed by freeze-dying under –4 °C. The Juglone/RGO electrode was finally obtained after compression treatment under a stress of 10 MPa. The mass fraction was controllable between 4.8% and 31.5% by simply adjusting the Juglone concentration between 0.5 and 3 g L^{-1}. $Na_3V_2(PO_4)_3$/C was prepared through a simple solid phase synthesis as reported.[76]

Characterization: The morphologies were observed using a JEOL JSM-7001F field-emission scanning electron microscope (FESEM). The elemental composition of the as-prepared electrodes was characterized using a JEOL JSM-7500F cold-FESEM with affiliated energy-dispersive X-ray diffraction spectroscopy. Transmission electron microscopy (TEM) and SAED were carried out on a JEOL JEM-2100F microscope. The mass fraction of Juglone was analyzed through thermogravimetric analysis at a heating rate of 10 °C min^{-1} under N_2 flow using Netzsch Sta449F3 thermal analyzer. The optical microscopy images were acquired using an Olympus BX51 microscope and the optical images were obtained using a Canon 600D camera. Raman spectroscopy measurements were performed on LabRAM HR800 system with an excitation wavelength of 633 nm. The silicon peak at 520 cm^{-1} was used as a reference. FTIR spectra were collected using a Bruker Vertex 70V instrument. The KBr pellets for FTIR measurements were prepared by pressing the powders/films and KBr powders with a stress of 10 MPa. X-ray photoelectron spectroscopy was carried out using a Thermo Scientific ESCALAB 250 XPS system. The spectra were referenced to the C 1s binding energy of 284.6 eV and analyzed using X-peak software. XANES experiments were performed at the Soft X-ray Spectroscopy station and Photoelectron Spectroscopy station of the Beijing Synchrotron Radiation Facility. The electron beam energy of the storage ring was 3.5 GeV with a maximum stored current of 300 mA. The spectra were normalized to the incident photon flux. Before the test, the charged/discharged electrodes were disassembled from coin-type cells in a N_2-filledglove box, washed with ethylene carbonate several times, and dried under vacuum.

Electrochemical Measurements: Cyclic voltammogram of Juglone in acetonitrile/deionized water mixed solution was captured by a three-electrode system, using a 1 M $NaClO_4$ electrolyte and Pt foils as both counter electrode and working electrode, as well as Ag/AgCl as reference electrode, with scan rates from 5 to 100 mV s^{-1}. The electrochemical performance of the Juglone/RGO electrodes was measured using CR2023 coin-type cells with pure Na metal foil as anode and 1 M $NaClO_4$ in ethylene carbonate and dimethyl carbonate (1:1, v/v) as electrolyte. Juglone/RGO hybridized electrodes were used as prepared without further treatment. The raw Juglone and RGO electrode was made by spreading fully mixed 80% powders, 10% carbon black, and 10% poly(vinylidene difluoride) onto a copper current collector and dried in a vacuum oven at 90 °C overnight. A porous glass fiber (GF/D) from Whatman was used as separator and 1 M $NaClO_4$ in ethylene carbonate and dimethyl carbonate (1:1 v/v) was used as the electrolyte for each battery. The cells were assembled in a N_2-filled glove box. The as prepared electrode was cut into pieces with dimension of 1.2 cm in length and 1.2 cm in width and one piece was used to calculate the mass of active material, and the other was used to assembly for sodium cell. The aluminum-pouch-type Na-ion batteries were prepared with $Na_3V_2(PO_4)_3$/C as cathode with 5:2 mass ratio in respect to Juglone/RGO anode and head-sealed at 160 °C. CV measurements were performed on electrochemical CHI 660D workstation at a scan rate of 1 mV s^{-1} in the range of 0 to 2.5 V. Charge/discharge measurements were carried out on CT 2001A Land battery testing systems (Jinnuo Electronics Co. Ltd., China) at different current densities in a potential range of 0.01–2.5 V versus Na/Na^+. EIS was performed on the CHI 660D electrochemical workstation at an open-circuit voltage, with an AC voltage of 5 mV, and in the frequency range of 100 kHz to 0.1 Hz.

Supporting Information

Supporting Information is available from the Wiley Online Library or from the author.

Acknowledgements

H.W. and P.H. contributed equally to this work. The authors acknowledge the funding support by National Natural Science Foundation of China (11079002).

Received: December 28, 2014
Revised: January 21, 2015
Published online: February 27, 2015

[1] S. W. Hwang, H. Tao, D. H. Kim, H. Cheng, J. K. Song, E. Rill, M. A. Brenckle, B. Panilaitis, S. M. Won, Y. S. Kim, Y. M. Song, K. J. Yu, A. Ameen, R. Li, Y. Su, M. Yang, D. L. Kaplan, M. R. Zakin, M. J. Slepian, Y. Huang, F. G. Omenetto, J. A. Rogers, *Science* **2012**, *337*, 1640.
[2] F. Cheng, J. Liang, Z. Tao, J. Chen, *Adv. Mater.* **2011**, *23*, 1695.
[3] S. Xin, Y.-X. Yin, Y.-G. Guo, L.-J. Wan, *Adv. Mater.* **2014**, *26*, 1261.
[4] X. Meng, X.-Q. Yang, X. Sun, *Adv. Mater.* **2012**, *24*, 3589.
[5] B. L. Ellis, P. Knauth, T. Djenizian, *Adv. Mater.* **2014**, *26*, 3368.
[6] Y. Zhai, Y. Dou, D. Zhao, P. F. Fulvio, R. T. Mayes, S. Dai, *Adv. Mater.* **2011**, *23*, 4828.
[7] J. Wang, N. Yang, H. Tang, Z. Dong, Q. Jin, M. Yang, D. Kisailus, H. Zhao, Z. Tang, D. Wang, *Angew. Chem.* **2013**, *125*, 6545.
[8] X. Jia, Z. Chen, X. Cui, Y. Peng, X. Wang, G. Wang, F. Wei, Y. Lu, *ACS Nano* **2012**, *6*, 9911.
[9] N. Yabuuchi, K. Kubota, M. Dahbi, S. Komaba, *Chem. Rev.* **2014**, *114*, 11636.
[10] K. Vuorilehto, *J. Appl. Electrochem.* **2003**, *33*, 15.
[11] W.-J. Li, S.-L. Chou, J.-Z. Wang, H.-K. Liu, S.-X. Dou, *Nano Lett.* **2013**, *13*, 5480.
[12] X. Cao, Y. Shi, W. Shi, X. Rui, Q. Yan, J. Kong, H. Zhang, *Small* **2013**, *9*, 3433.

[13] S. Han, D. Wu, S. Li, F. Zhang, X. Feng, *Adv. Mater.* **2014**, *26*, 849.
[14] S. Yuan, X. Huang, D. Ma, H. Wang, F. Meng, X. Zhang, *Adv. Mater.* **2014**, *26*, 2284.
[15] Y. Tang, Y. Zhang, J. Deng, J. Wei, H. L. Tam, B. K. Chandran, Z. Dong, Z. Chen, X. Chen, *Adv. Mater.* **2014**, *26*, 6111.
[16] H. Chen, M. Armand, G. Demailly, F. Dolhem, P. Poizot, J. M. Tarascon, *ChemSusChem* **2008**, *1*, 348.
[17] L. Zhang, Z. Liu, G. Cui, L. Chen, *Prog. Polym. Sci.* DOI: 10.1016/j.progpolymsci.2014.09.003.
[18] I. Kovalenko, B. Zdyrko, A. Magasinski, B. Hertzberg, Z. Milicev, R. Burtovyy, I. Luzinov, G. Yushin, *Science* **2011**, *334*, 75.
[19] J. L. Rouge, B. E. Eaton, D. L. Feldheim, *Energy Environ. Sci.* **2011**, *4*, 398.
[20] M. Armand, J. M. Tarascon, *Nature (London)* **2008**, *451*, 652.
[21] T. Janoschka, M. D. Hager, U. S. Schubert, *Adv. Mater.* **2012**, *24*, 6397.
[22] M.-R. Gao, Y.-F. Xu, J. Jiang, S.-H. Yu, *Chem. Soc. Rev.* **2013**, *42*, 2986.
[23] C. Liu, F. Li, L.-P. Ma, H.-M. Cheng, *Adv. Mater.* **2010**, *22*, E28.
[24] D. Larcher, J. M. Tarascon, *Nat. Chem.* **2015**, *7*, 19.
[25] O. Inganäs, S. Admassie, *Adv. Mater.* **2014**, *26*, 830.
[26] J. Cabana, L. Monconduit, D. Larcher, M. R. Palacín, *Adv. Mater.* **2010**, *22*, E170 .
[27] H. Tang, J. Wang, H. Yin, H. Zhao, D. Wang, Z. Tang, *Adv. Mater.* **2015**, *27*, 1117.
[28] S. K. Kim, Y. K. Kim, H. Lee, S. B. Lee, H. S. Park, *ChemSusChem* **2014**, *7*, 1094.
[29] G. Milczarek, O. Inganas, *Science* **2012**, *335*, 1468.
[30] M. Armand, S. Grugeon, H. Vezin, S. Laruelle, P. Ribiere, P. Poizot, J. M. Tarascon, *Nat. Mater.* **2009**, *8*, 120.
[31] S. Wang, L. Wang, K. Zhang, Z. Zhu, Z. Tao, J. Chen, *Nano Lett.* **2013**, *13*, 4404.
[32] J. Hong, M. Lee, B. Lee, D. H. Seo, C. B. Park, K. Kang, *Nat. Commun.* **2014**, *5*, 5335.
[33] M. Lee, J. Hong, H. Kim, H. D. Lim, S. B. Cho, K. Kang, C. B. Park, *Adv. Mater.* **2014**, *26*, 2558.
[34] M. Lee, J. Hong, D. H. Seo, D. H. Nam, K. T. Nam, K. Kang, C. B. Park, *Angew. Chem. Int. Ed.* **2013**, *52*, 8322.
[35] Y. J. Kim, W. Wu, S. E. Chun, J. F. Whitacre, C. J. Bettinger, *Proc. Natl. Acad. Sci. USA* **2013**, *110*, 20912.
[36] P. Poizot, F. Dolhem, *Energy Environ. Sci.* **2011**, *4*, 2003.
[37] H. Tang, H. Yin, J. Wang, N. Yang, D. Wang, Z. Tang, *Angew. Chem. Int. Ed.* **2013**, *125*, 5695.
[38] X. Han, C. Chang, L. Yuan, T. Sun, J. Sun, *Adv. Mater.* **2007**, *19*, 1616.
[39] T. Nokami, T. Matsuo, Y. Inatomi, N. Hojo, T. Tsukagoshi, H. Yoshizawa, A. Shimizu, H. Kuramoto, K. Komae, H. Tsuyama, J. Yoshida, *J. Am. Chem. Soc.* **2012**, *134*, 19694.
[40] C. Luo, R. Huang, R. Kevorkyants, M. Pavanello, H. He, C. Wang, *Nano Lett.* **2014**, *14*, 1596.
[41] Q. Su, S. Pang, V. Alijani, C. Li, X. Feng, K. Müllen, *Adv. Mater.* **2009**, *21*, 3191.
[42] B. Genorio, K. Pirnat, R. Cerc-Korosec, R. Dominko, M. Gaberscek, *Angew. Chem. Int. Ed.* **2010**, *49*, 7222.
[43] L. Zhao, W. Wang, A. Wang, K. Yuan, S. Chen, Y. Yang, *J. Power Sources* **2013**, *233*, 23.
[44] Z. Song, Y. Qian, X. Liu, T. Zhang, Y. Zhu, H. Yu, M. Otani, H. Zhou, *Energy Environ. Sci.* **2014**, *7*, 4077.
[45] Z. Song, H. Zhan, Y. Zhou, *Angew. Chem. Int. Ed.* **2010**, *49*, 8444.
[46] Y. Hanyu, T. Sugimoto, Y. Ganbe, A. Masuda, I. Honma, *J. Electrochem. Soc.* **2013**, *161*, A6.
[47] Z. Zhu, M. Hong, D. Guo, J. Shi, Z. Tao, J. Chen, *J. Am. Chem. Soc.* **2014**, *136*, 16461.
[48] Y. Morita, S. Nishida, T. Murata, M. Moriguchi, A. Ueda, M. Satoh, K. Arifuku, K. Sato, T. Takui, *Nat. Mater.* **2011**, *10*, 947.
[49] A. Shimizu, H. Kuramoto, Y. Tsujii, T. Nokami, Y. Inatomi, N. Hojo, H. Suzuki, J. Yoshida, *J. Power Sources* **2014**, *260*, 211.
[50] L. David, R. Bhandavat, G. Singh, *ACS Nano* **2014**, *8*, 1759.
[51] J. Billaud, R. J. Clément, A. R. Armstrong, J. Canales-Vázquez, P. Rozier, C. P. Grey, P. G. Bruce, *J. Am. Chem. Soc.* **2014**, *136*, 17243.
[52] Y. Fang, L. Xiao, J. Qian, X. Ai, H. Yang, Y. Cao, *Nano Lett.* **2014**, *14*, 3539.
[53] W. Li, S.-L. Chou, J.-Z. Wang, J. H. Kim, H.-K. Liu, S.-X. Dou, *Adv. Mater.* **2014**, *26*, 4037.
[54] Y. Park, D. S. Shin, S. H. Woo, N. S. Choi, K. H. Shin, S. M. Oh, K. T. Lee, S. Y. Hong, *Adv. Mater.* **2012**, *24*, 3562.
[55] Y. J. Kim, W. Wu, S.-E. Chun, J. F. Whitacre, C. J. Bettinger, *Adv. Mater.* **2014**, *26*, 6572.
[56] X. Zhang, Y. Feng, S. Tang, W. Feng, *Carbon* **2010**, *48*, 211.
[57] L. Wang, K.-Y. Pu, J. Li, X. Qi, H. Li, H. Zhang, C. Fan, B. Liu, *Adv. Mater.* **2011**, *23*, 4386.
[58] J. Björk, F. Hanke, C.-A. Palma, P. Samori, M. Cecchini, M. Persson, *J. Phys. Chem. Lett.* **2010**, *1*, 3407.
[59] S.-Y. Ju, J. Doll, I. Sharma, F. Papadimitrakopoulos, *Nat. Nanotechnol.* **2008**, *3*, 356.
[60] S.-Y. Ju, W. P. Kopcha, F. Papadimitrakopoulos, *Science* **2009**, *323*, 1319.
[61] X. Cao, D. Qi, S. Yin, J. Bu, F. Li, C. F. Goh, S. Zhang, X. Chen, *Adv. Mater.* **2013**, *25*, 2957.
[62] J. Shen, Y. Hu, M. Shi, X. Lu, C. Qin, C. Li, M. Ye, *Chem. Mater.* **2009**, *21*, 3514.
[63] J. Jin, P. Hassanzadeh, G. Perotto, W. Sun, M. A. Brenckle, D. Kaplan, F. G. Omenetto, M. Rolandi, *Adv. Mater.* **2013**, *25*, 4482.
[64] Y.-X. Wang, S.-L. Chou, H.-K. Liu, S.-X. Dou, *Carbon* **2013**, *57*, 202.
[65] Y. J. Oh, J. J. Yoo, Y. I. Kim, J. K. Yoon, H. N. Yoon, J.-H. Kim, S. B. Park, *Electrochim. Acta* **2014**, *116*, 118.
[66] H.-K. Zhang, H. Lu, J. Wang, J.-T. Zhou, M. Sui, *Environ. Sci. Technol.* **2014**, *48*, 12876.
[67] C. Cheng, S. Nie, S. Li, H. Peng, H. Yang, L. Ma, S. Sun, C. Zhao, *J. Mater. Chem. B* **2013**, *1*, 265.
[68] J. Zhong, J.-J. Deng, B.-H. Mao, T. Xie, X.-H. Sun, Z.-G. Mou, C.-H. Hong, P. Yang, S.-D. Wang, *Carbon* **2012**, *50*, 335.
[69] L. S. Zhang, W. D. Wang, X. Q. Liang, W. S. Chu, W. G. Song, W. Wang, Z. Y. Wu, *Nanoscale* **2011**, *3*, 2458.
[70] J. Zhong, L. Song, J. Chiou, C. Dong, X. Liang, D. Chen, S. Xie, W.-F. Pong, C. Chang, J. Guo, Z. Wu, *Appl. Phys. Lett.* **2010**, *96*, 213112.
[71] W. Ai, Z. Du, Z. Fan, J. Jiang, Y. Wang, H. Zhang, L. Xie, W. Huang, T. Yu, *Carbon* **2014**, *76*, 148.
[72] E. Yoo, J. Kim, E. Hosono, H.-S. Zhou, T. Kudo, I. Honma, *Nano Lett.* **2008**, *8*, 2277.
[73] C. Wang, D. Li, C. O. Too, G. G. Wallace, *Chem. Mater.* **2009**, *21*, 2604.
[74] X. Huang, Z. Zeng, Z. Fan, J. Liu, H. Zhang, *Adv. Mater.* **2012**, *24*, 5979.
[75] S. Yin, Y. Zhang, J. Kong, C. Zou, C. M. Li, X. Lu, J. Ma, F. Y. C. Boey, X. Chen, *ACS Nano* **2011**, *5*, 3831.
[76] S. Li, Y. Dong, L. Xu, X. Xu, L. He, L. Mai, *Adv. Mater.* **2014**, *26*, 3545.